

# Muon identification in a compact single-layered water Cherenkov detector and gamma/hadron discrimination using Machine Learning techniques

R. Conceição<sup>1,2</sup>, B.S. González<sup>1,2,3</sup>, A. Guillén<sup>3</sup>, M. Pimenta<sup>1,2</sup>,  
B. Tomé<sup>1,2</sup>

<sup>1</sup> LIP, Av. Prof. Gama Pinto, 2, P-1649-003 Lisbon, Portugal

<sup>2</sup> Instituto Superior Técnico (IST), Universidade de Lisboa, Av. Rovisco Pais 1, 1049-001, Lisbon, Portugal

<sup>3</sup> Computer Architecture and Technology Department, University of Granada, Granada, Spain

Received: date / Accepted: date

**Abstract** The muon tagging is an essential tool to distinguish between gamma and hadron-induced showers in wide field-of-view gamma-ray experiments. In this work, it is shown that a good muon tagging (and counting) can be achieved using a water Cherenkov detector with a reduced water volume and 4 PMTs, provided that the PMT signal spatial and time patterns are interpreted by an analysis based on Machine Learning. The developed analysis has been tested for different shower and array configurations. The output of the ML analysis, the probability of having a muon in the WCD station, has been used to notably discriminate between gamma and hadron induced showers with  $S/\sqrt{B} \sim 4$  for shower with energies  $E_0 \sim 1$  TeV.

**Keywords** High Energy gamma rays · Wide field-of-view observatories · Water Cherenkov Detectors · Muon identification · Gamma/hadron discrimination · Machine Learning

## 1 Introduction

The study of gamma-rays is crucial to investigate our surrounding Universe. Their neutral nature allows them to cover long distances along the Universe without being deflected by magnetic fields. Thus, the detection of gamma-rays can be used to track emitting astrophysical sources. In particular, gamma-rays ranging from  $\sim 100$  GeV and few hundred TeV, known as very high-energy (VHE) gamma-rays, are very interesting to investigate some of the most extreme non-thermal events taking place in the Universe, sometimes related to stellar explosions or with the presence of compact objects like

neutron stars or supermassive black holes [1]. Furthermore, not only is gamma-rays detection important for identifying astrophysical emitting sources, but it could also be essential in proving the existence of new physics at fundamental scales beyond the standard model of particle physics [2].

The direct detection of gamma-rays is only possible using artificial satellite-borne instruments [3]. Nevertheless, above a few hundreds of GeV, the gamma-ray flux becomes too small and only ground-based experiments can indirectly detect this kind of radiation. Indirect detection techniques take advantage of the secondary shower of particles, known as Extensive Air Showers (EAS), produced by the interaction of the gamma-ray with the Earth's atmosphere to infer their direction and energy. However, even though indirect methods are very effective at the VHE energy region, a significant drawback is that one has to deal with an enormous hadronic background produced by the cosmic-rays continuously reaching the Earth. At the sub-TeV region, the rejection of cosmic-rays can be done by exploring the patterns of the secondary particles reaching the ground [4,5]. At the TeV energy range, muons begin to appear in significant quantities in hadronic showers. Therefore, the detection of muons provides an important tool to efficiently separate between gamma and hadronic extensive air showers [6,7].

The main aim of this work is to prove that a dedicated design of the water Cherenkov detector (WCD) combined with state-of-the-art machine learning techniques can be used to identify muons and with it provide a good gamma/hadron discrimination. The achievement of this goal could be used to enhance future generation detector's efficiency and can lead to investment savings

<sup>a</sup>e-mail: borjasg@lip.pt

due to the reduction of the amount of water needed at such high altitude.

Hence, for the present study, we propose the use of an EAS wide field-of-view array composed of water Cherenkov detectors (Section 2). The signals time traces recorded by the WCDs will be analysed to distinguish between muons and electromagnetic shower secondary particles (electrons, positrons and photons) by means of a *Convolutional Neural Network* (Section 4). Afterwards, the information about muons found by the algorithm was used to carry out a gamma/hadron discrimination (Section 5) and estimate the number of muons in hadronically induced showers (Section 6). Finally, a discussion on the performance for inclined shower events and a sparser detector array is presented in Section 7, followed by the conclusions.

## 2 WCD configuration

Several approaches to identify muons in ground-based wide field-of-view gamma-ray experiments have been tried or suggested over time. One of the most successful approaches comes from the HAWC experiment [8]. The HAWC tanks contain a large volume of water and black walls. This can be used to attenuate the electromagnetic particles whilst muons traverse the whole detector giving a large signal and an unmistakable signature. This detector, although highly successful on the TeV energy range, has a limited performance in the sub-TeV energies and its massive amount of water does not make it a good candidate to place it at higher altitude (one of the most effective ways to lower the energy threshold).

Another option would be to use dedicated muon detectors, buried or shielded, as it is being done in LHASSO [9] or simply below the water tank, as proposed in the MARTA project [10]. These hybrid experiments have many advantages as the shower components can be scrutinised by independent detectors. However, it also dramatically increases the cost of the project. Note that VHE gamma-ray experiments such as LHAASO or the future Southern Wide field Gamma-ray Observatory (SWGGO) [11], need to cover huge areas up to  $1 \text{ km}^2$  and muons are relatively scarce for  $\sim \text{TeV}$  showers.

In this work, we aim to explore another via that uses solely a single-layered WCD with 4 PMTs (see Figure 1). The rationale behind this concept is that muons will cross the whole detector and as such, the direct Cherenkov light, produced along with its traversal, will reach only a portion of the WCD floor. Contrary, photons and electrons give origin to electromagnetic showers inside the station, creating a broader Cherenkov light pool.

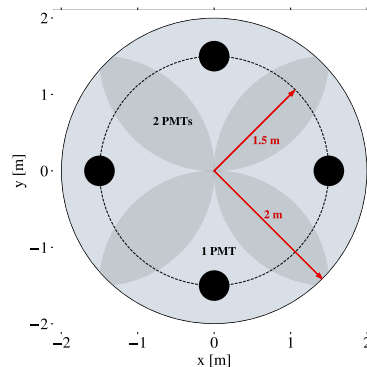


Figure 1: Single-layered WCD design. A dark circular area with a radius of 1.5 m was drawn around each 8-inch PMT (represented as black circles). Taking into account the height of this WCD, the direct Cherenkov light of a vertical muon that crosses the WCD through one of these areas should be detected by its correspondent PMT (it could be detected by two PMTs in the case that a muon crosses the station through the intersection of two dark areas).

Moreover, muons travel mostly alone while electromagnetic particles arrive in bulks, which further supports this signal asymmetry view.

By considering vertically crossing muons and taking into account that the Cherenkov angle for relativistic muons in water is  $\sim 41^\circ$ , one can see that to guarantee that the Cherenkov light pool is seen by only 2 PMTs at most (maximise the signal asymmetries), one should choose the following WCD dimensions:

- Tank diameter 4 m;
- Tank height 1.7 m;
- PMT distance to the WCD centre of 1.5 m.

The WCD diameter is an ad-hoc parameter, chosen as a good compromise between the segmentation of the experiment and its cost. It is worth noting that these dimensions also guarantee that the WCD has a good light collection uniformity independently of the entry point of the muon. The walls of this WCD should be white diffusive to maximise the signal collection and effectively lower the energy threshold. Analyses, such as the shower geometry reconstruction that need the shower arrival time with a high time resolution, can be done by collecting the first peak associated with directing light production (see for instance the signal time trace of PMT 3 in Figure 2). This first peak appears typically within the first 10 ns to the signal starting time trace,  $T_0$ .

The full analyses of the detector performance of this WCD unit with four PMTs is out of the scope of this

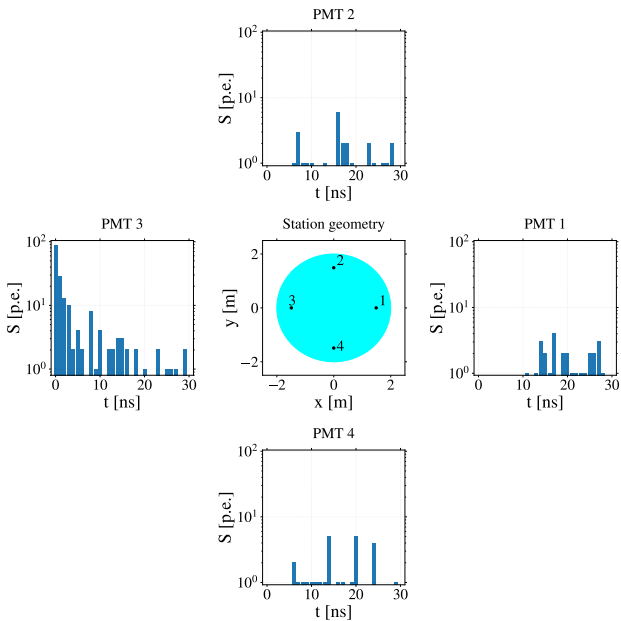


Figure 2: Single-layered WCD crossed by a single relativistic muon. The WCD drawing is surrounded by the correspondent PMT signal time traces.

paper. Here, we intend to show that the signal asymmetry and the analysis of the complex PMT signal time trace can be used in combination with machine learning algorithms to identify the presence of muons in it.

### 3 Simulation and analysis strategy

#### 3.1 Simulations

The extensive air showers used in this work were simulated with CORSIKA (version 7.5600) [12] and the detector response using the Geant4 toolkit (with version 4.10.05.p01) [13, 14, 15].

To train and assess the performance of the machine learning algorithms it was used proton-induced shower simulations with energies  $E_0 \in [4; 6]$  TeV. This energy range was selected to ensure enough quantity of stations with only muons (without other particles crossing the WCD), and also stations with muons and some electromagnetic contamination to evaluate the resilience of the models. The showers were generated following a  $E_0^{-1}$  spectra, an azimuth angle uniformly distributed, and a zenith angle  $\theta_0 \in [5^\circ; 15^\circ]$  (vertical events) and  $\theta_0 \in [25^\circ; 35^\circ]$  (inclined events). The experiment observation level was set at 5200 m above the sea level.

Two array configurations of WCDs are compared to investigate the impact of the WCDs distribution at ground in the results for inclined showers. Their para-

eters were chosen for being one of the possibilities for SWGO. The array matrices cover an area of roughly  $80\,000\text{ m}^2$  and have the following characteristics:

- a dense array which is composed of 5720 WCDs nearly touching each other (fill factor of  $\sim 80\%$ );
- a sparse array with 1906 WCDs with a minimum separation of  $\approx 12\text{ m}$ . This array was built by removing stations such that no WCD has a neighbour station closer than its own diameter.

In Sections 5 and 6, the identification of muons is used to perform the gamma/hadron discrimination and to estimate the number of muons in hadronic showers. A particular set of simulations was derived in order to enable a sensible comparison between gamma and hadron events. Gamma-induced showers were generated with energies between  $E_0 \in [1; 1.6]$  TeV, while proton-induced showers were simulated for energies between 700 GeV and 6 TeV. The zenith angles for both are comprised between  $5^\circ - 15^\circ$ . Afterwards, a cut on the total measured WCD signal at the ground is applied to emulate a typical energy reconstruction (see Figure 3):

$$S_T \in [\langle S_{T,\gamma} \rangle - \sigma_{S_{T,\gamma}}; \langle S_{T,\gamma} \rangle + \sigma_{S_{T,\gamma}}] = [0.4; 1.8] \cdot 10^5 \text{ p.e.}$$

where  $S_T$  is the total signal at ground using all the WCDs,  $\langle S_{T,\gamma} \rangle$  and  $\sigma_{S_{T,\gamma}}$  are the average and standard deviation respectively of the distribution for  $S_T$  in gamma-ray events. Since the events were generated with a  $E_0$  spectra, the distributions were weighted before applying the cut on the signal and during the entire experimentation in section 5. The weights  $E_{0,\gamma}^{-1}$  and  $E_{0,p}^{-2}$  were applied to ensure a realistic power law spectrum of energies (expected to be  $\sim E_{0,\gamma}^{-2}$  and  $\sim E_{0,p}^{-3}$ ).

To sum up, in Tables 1 and 2 we describe the data sets used to train and assess the artificial neural networks. It should be noted that some considerations were taken into account before building these data sets. To avoid events where the muon partially crossed the station, only stations with more than 300 photoelectrons (p.e.) were used during the experimentation (train and test of the machine learning algorithms). Only *Single Muons*<sup>1</sup> (as well as stations without muons) were considered during the training process in order to provide representative muon samples to the algorithm. All kind of stations with muons are considered for the test sets. A second training data set was built to train again the neural network with inclined events (using the same configuration of the algorithm that was optimised for vertical events).

<sup>1</sup>WCD with only one muon crossing it and nothing else

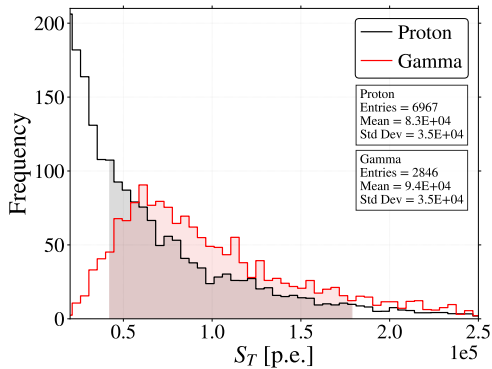


Figure 3: Signal at the ground of gamma and proton induced EAS used in Section 5. The area below the selected events was filled in red for gammas and grey for protons. The statistical data showed in this figure corresponds only to the selected events.

	$\theta_0 \in [5^\circ; 15^\circ]$		$\theta_0 \in [25^\circ; 35^\circ]$
	Training	Validation	Training
EAS	2 000 (80%)	2 000 (20%)	655
S.M. stations	13 795	3 449	5 472
E.M. stations	272 006	68 001	85 130
Instances	285 801	71 450	90 602
Muonic prop.	4.83 %	4.83 %	6.04 %

Table 1: Number of stations with *Single Muons* (S.M. stations) and without muons (E.M. stations) of the training data sets. Data sets created using vertical ( $\theta_0 \in [5^\circ; 15^\circ]$ ) and inclined ( $\theta_0 \in [25^\circ; 35^\circ]$ ) showers with primary energy  $E_0 \in [4; 6]$  TeV and the dense array. A validation data set was created using a 20% of the stations from the original 2 000 vertical EAS.

Primary	Array	$E_0$ (TeV)	$\theta_0$ ( $^\circ$ )	EAS	Stations with All Muons	Stations without muons
Proton	Dense	[4; 6]	[5; 15]	1 693	57 283	289 411
Proton	Dense	[4; 6]	[25; 35]	281	7 601	34 738
Proton	Sparse	[4; 6]	[25; 35]	936	8 452	40 933
Proton	Dense	[0.7; 6]	[5; 15]	6 967	107 579	379 421
Gamma	Dense	[1; 1.6]	10	2 846	263	174 103

Table 2: Description of the test data sets.

### 3.2 Analysis strategy

The objective function defined for this problem is the probability,  $P_\mu^{(i)} \in [0, 1]$ , that a muon has passed through the WCD ( $i$ ) whose signal is being analysed. In such a way, the method is intended to be able to tag contaminated events where not only muons have crossed through the station.

To carry out this identification of stations with muons we propose the use of variables based solely on the WCD signal [16]. With the following variables we aim to explore both temporal (patterns in the signal time traces) and spatial (asymmetry in the PMTs' integrals) features:

- Normalised signal time trace of each PMT.
- Integral of each PMTs signal time trace.
- Cherenkov light measured in the WCD (sum of the four PMTs' signal trace integrals).
- Normalised integral of each PMTs signal time trace.

The normalisation was done using the total Cherenkov light measured by the four PMTs during the time window considered for the variable that is going to be normalised. Note that the normalised signal traces contain the first 30 nanoseconds to explore features from both direct the Cherenkov light and the reflections, while the rest of variables considered only the direct Cherenkov light (first 10 nanoseconds).

### 3.3 Convolutional Neural Networks: design, training and optimisation

Convolutional Neural Networks (CNNs) have become a standard in many machine learning applications. CNNs are feed-forward Artificial Neural Networks which combine two main blocks of hidden layers: *convolutional layers* and *fully-connected layers*. By using these layers, the CNN is able to fuse the processes of extracting features from data and perform a classification or regression. In this work we use a 1-dimensional Convolutional Neuronal Network to extract complex features from the signals traces of the PMTs and combine it with the spatial features (integrals). With it, we define a regression problem to provide the probability  $P_\mu^{(i)}$ .

The configuration of the algorithm was optimised evaluating possible values with the validation data set for vertical showers. One input channel of data was established for each PMT signal trace. Three convolutional layers were set to study the signal time traces. ReLU activation function is used and the number of filters in these layers was 20, 15 and 10. The size of the filters was established by taking into consideration the mean signal traces of the stations muons, which reveals that the first pulse of direct Cherenkov light usually appears within the first 2 nanoseconds. Therefore, small filters of size 2 are introduced, including a stride equal to two in the first filter to emphasise the first maximum of signal. Afterwards, three dense layers are introduced to perform the regression using the previous signal features and the spatial variables. These layers are com-

posed of 30, 15 and 10 neurons respectively. A final output layer with a single neuron was used to compute the final probability. Sigmoid activation function was used for the three dense layers and final neuron. Adam learning algorithm was used during the training stage, which is a stochastic gradient-based method broadly applied in many deep learning applications. The adjustment of its parameters was done following those recommended in [17], that is:  $(\beta_1, \beta_2) = (0.9, 0.999)$  and  $\varepsilon = 10^{-7}$ . Finally, the model was trained during 200 epochs with a batch size of 512 and a learning rate of  $10^{-3}$ . Python 3.7 and Keras were used as the framework of the entire study.

Note that the stations with muons constitute roughly a 5 % of the total (see Table 1). Therefore, the class ratio must be balanced before training [18]. A random oversampling technique was applied to the training set, creating new samples of stations with muons by randomly repeating those available in the data set. Finally, the class ratio was adjusted to  $N_{\mu}/N_{e.m.} = 0.5$ . The class ratio was not completely balanced in order to avoid false positives.

#### 4 Discrimination of muons in the WCD

To assess the performance of the method, the probability  $P_{\mu}^{(i)}$  will be measured in stations with and without muons. Since the algorithm was trained using only Single Muons, the stations with muons will be distributed in different subclasses to study the impact of the electromagnetic contamination in the probability.

The simulation only provided the amount of signal produced in the WCD ( $S_T$ ), but not the two components ( $S_{e.m.}$  and  $S_{\mu}$ ) separately as it does with the energy. Therefore, a relation between the signal produced in events with Single Muons and its energy was calibrated. This allowed us to estimate the signal produced by the muon by means of its energy. Afterwards, the proportion of electromagnetic induced signal  $s_{e.m.} \in [0; 1]$  was computed using the equation (1).

$$s_{e.m.} = \frac{S_T - S_{\mu}}{S_T} = \frac{S_{e.m.}}{S_T} \quad (1)$$

In Figure 4 it is shown the normalised inverse cumulative function for the probability  $P_{\mu}^{(i)}$  measured in stations from proton induced events with  $E_0 \in [4, 6]$  TeV and  $\theta_0 \in [5^{\circ}; 15^{\circ}]$ . Most events with muons and low electromagnetic contamination were correctly identified, where roughly a 70% have a probability  $P_{\mu}^{(i)} \geq 0.5$ . For higher electromagnetic contamination we get lower  $P_{\mu}^{(i)}$  values. Approximately a 40% and a 20% of the events with  $s_{e.m.} \in [0.1; 0.2]$  and  $s_{e.m.} \in [0.2; 0.5]$

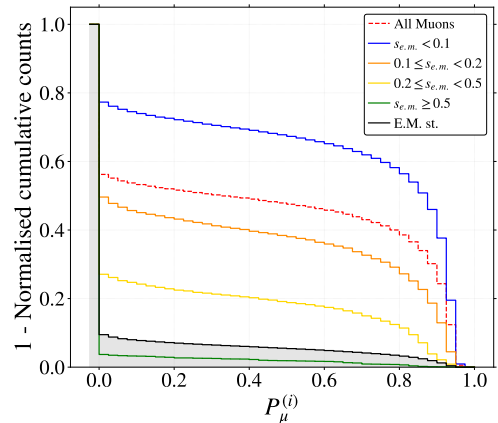


Figure 4: Impact of electromagnetic contamination using the normalised inverse cumulative function for the probability  $P_{\mu}^{(i)}$ . Stations from proton-induced events with  $E_0 \in [4, 6]$  TeV and  $\theta_0 \in [5^{\circ}; 15^{\circ}]$ .

respectively were identified with  $P_{\mu}^{(i)} \geq 0.5$ . Almost no probability is attributed to those events where most of the signal was not originated by the muon. This low probability may be justified given that these events involve a high electromagnetic signal, which added to the one caused by the muon, can cause a lower asymmetry among the PMTs signals. Taking into account all possible stations with muons, around a 50% of the stations had  $P_{\mu}^{(i)} \geq 0.5$ . This result proves that the algorithm was able to learn the main characteristics of the muonic signal from the *Single Muons* events, so that the neural network is able to identify most single muons events and some contaminated events that share some of their features with single muons. Finally, less than a 10% of the stations without muons had a probability  $P_{\mu}^{(i)} > 0$ .

#### 5 Gamma/hadron discrimination strategies

In this section, we propose a gamma/hadron discrimination strategy which relies on the use of solely the information extracted in the previous sections at the WCD station level,  $P_{\mu}^{(i)}$ . This information should be combined at the shower event. A simple and intuitive observable was created for this purpose in equation (2).

$$P_{\mu} = \sum_{i=1}^{N_S} P_{\mu}^{(i)} \quad (2)$$

As seen before,  $P_{\mu}^{(i)}$  is the probability, derived by the ML method, that the WCD station  $i^{\text{th}}$  was crossed by a muon, and  $N_S$  is the total number of WCD stations with more than 300 p.e. in the shower event.

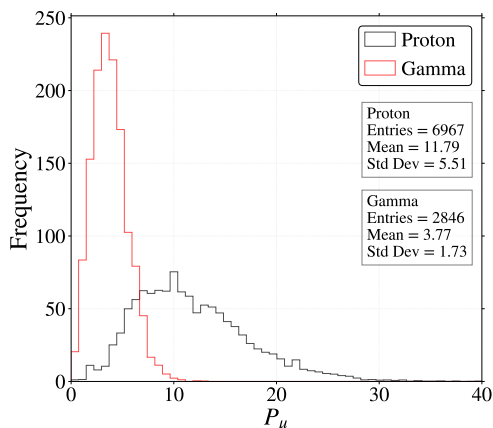


Figure 5: Distribution of the probability  $P_\mu$  after evaluating all the stations of the array for gamma and proton induced showers with energies  $E_0 \in [1; 1.6]$  TeV and  $E_0 \in [0.7; 6]$  TeV respectively.

The observable established in equation (2) is tested for proton and gamma induced showers in Figure 5. As expected, larger values are found when evaluating those events which have muons, i.e., proton initiated air showers. Moreover, it can be seen that by adequately choosing a cut on  $P_\mu$ , the gamma-induced showers can be efficiently separated from the ones generated by protons. It should be noted that there could be proton events of energy  $E_0 \sim 0.7$  TeV with few or without muons, leading to low probabilities  $P_\mu$ .

A proxy to a gamma-ray experiment flux sensitivity can be obtained evaluating  $S/\sqrt{B}$ , where  $S$  and  $B$  are the selection efficiency for gamma-rays and the background (protons induced events), respectively.

In Figure 6 it is shown the  $S/\sqrt{B}$  of the simulated instrument using this method. The motivation for sampling only stations far away from the shower core arises from shower physics considerations. On the one hand, muons can be produced in hadronically developing showers with high transverse momentum, and consequently falling far away from the shower core. On the other, the bulk electromagnetic shower component is much higher near the shower core. A cut on the probability  $P_\mu^{(i)}$  was also tried without much difference on the results. A  $S/\sqrt{B}$  of roughly 4 was found when fixing the selection efficiency for gammas to  $S = 0.6$ . The obtained value is similar to the one quoted in other experiments such as LATTES<sup>2</sup> [19] and HAWC [20], but using a significantly smaller WCD than HAWC.

<sup>2</sup>Simulation study in similar conditions.

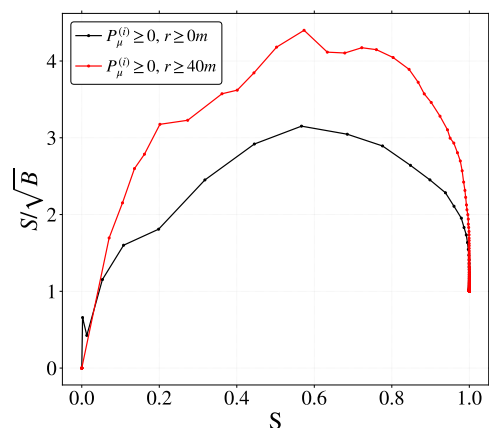


Figure 6: Evaluation of the  $S/\sqrt{B}$  achieved using selected stations as a function of the selection efficiency  $S$  for gamma-rays.

## 6 Muon counting in proton-induced events

In the previous section, a gamma/hadron separation was pursued. For that, it was enough identifying a certain quantity of the muons that reached stations. Nevertheless, muon counting capabilities when analysing hadronic induced EAS are of great interest.

To prove that the discrimination achieved in Sections 4 and 5 comes from the fact that we are measuring muons and not any other shower feature, we decided to plot the correlation between  $P_\mu$  and the number of muons crossing through the WCDs stations  $N_\mu$  (this time we include events whose signal is lower than 300 p.e.) for each proton shower event. The result is shown in Figure 7 and it can be seen that there is a linear relationship between both variables. It should be noted that the ML method was not trained to count muons but instead to simply find them. However, for proton showers with energies  $E_0 \sim 1$  TeV the number of WCD stations with more than one muon is negligible, and as such,  $P_\mu$  is in this conditions a good proxy for  $N_\mu$ .

It is then possible to calibrate it and estimate the number of muons by measuring the probability of having muons in all the stations. As such, the average probability  $P_\mu$  assigned by the method to showers with the same number of muons  $N_\mu$  is computed (see Figure 7). Due to the scarce number of events with  $N_\mu \geq 40$ , a unique weighted mean value is considered taking into account all of them. We must take into account that, since we need to identify all the muons, no cuts on the distance to the shower core or on the probability  $P_\mu$  are applied during this analysis.

Finally, in equation (3) it is described the calibration of the estimated number of muons  $\hat{N}_\mu$  as a function of

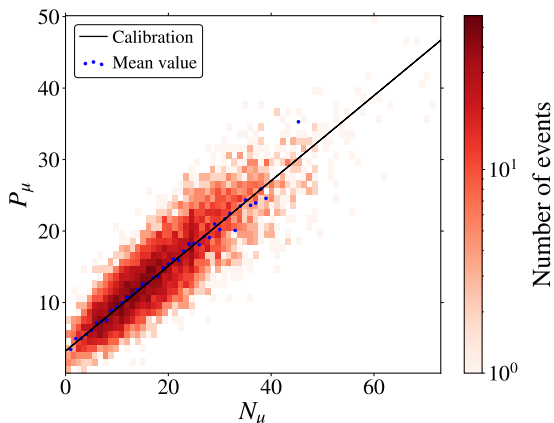


Figure 7: Calibration of the relationship between  $N_\mu = \sum_{i=0}^{N_S} N_\mu^{(i)}$  and  $P_\mu = \sum_{i=0}^{N_S} P_\mu^{(i)}$  using proton induced air showers.

the amount of probability  $P_\mu$  measured. The intercept of the calibration could be understood as the average probability from the stations without muons. In fact, this value  $\sim 3$  is similar to the mean probability  $P_\mu$  found in gamma-ray induced events of similar signal at the ground (see Figure 5) where the presence of muons is very scarce.

$$\hat{N}_\mu = 1.67 \cdot P_\mu - 3.22 \quad (3)$$

In Figure 8 it is shown both the resolution and the bias of the calibration proposed in equation (3). For events with  $N_\mu > 10$  resolutions of about a 20% and a bias of just a few % were found. The resolution of the method for events with  $N_\mu \geq 20$  can be adjusted to a function  $1.06/\sqrt{N_\mu} + 0.02$ . Therefore, the intrinsic resolution of the method is estimated to be just a 2%. In view of these results, it can be seen that the samples with few muons are dominated by the electromagnetic noise, then larger fluctuations are found. As a consequence, as we increase the number of stations with muons, the electromagnetic contribution becomes a small portion of the overall probability  $P_\mu$ , which leads to more precise measurements.

## 7 Discussion

The proposed method has proven to be effective when identifying muons under the same circumstances used during the training stage:  $E_0 \sim 4$  TeV and  $\theta_0 \sim 10^\circ$ . However, the possible degradation of the method performance in other scenarios must be discussed. An important factor is the inclination of the events and its

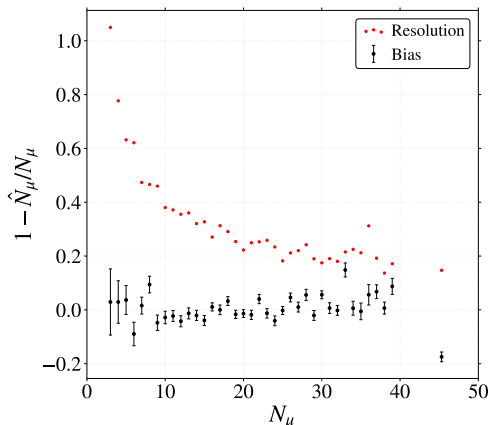


Figure 8: Resolution and bias of the calibration between  $N_\mu$  and  $P_\mu$ .

impact in the results depending on the array configuration (dense or sparse).

To assess the impact of the shower zenith angle  $\theta_0$  in the muon tagging, proton-induced events with  $\theta_0 \in [25^\circ; 35^\circ]$  were tested. Using the algorithm optimised for vertical showers it was found that roughly a 25% of All Muons had a probability  $P_\mu^{(i)} \geq 0.5$ . The result for stations without muons was similar to the one achieved using vertical showers. In view of this result, a CNN with the same configuration used for vertical showers was trained again using only inclined events (see Table 1 for more details).

In Figure 9 it is compared the normalised inverse cumulative function of the probability  $P_\mu^{(i)}$  for inclined showers (using the algorithm that was trained for these showers  $P_{\mu, \text{incl.}}^{(i)}$ ) and vertical showers (using the algorithm previously trained with vertical showers  $P_{\mu, \text{vert.}}^{(i)}$ ). Inclined showers are tested in both the dense and the sparse array. The newly trained algorithm had a very similar performance for both arrays considering stations with. Therefore, one can conclude that the performance of the muon tagging for these WCDs is not affected by the distance of the neighbour stations.

The proportion of each station class with probability  $P_\mu^{(i)} \geq 0.5$  was:  $\sim 70\%$  of slightly contaminated muons;  $\sim 55\%$  of All Muons; and  $\sim 10\%$  of the stations without muons. In comparison with the vertical events, a slight improvement was found when identifying All Muons whilst the performance with the stations without muons worsened. It should be noted that the CNN configuration was not optimised for inclined events, we just trained the algorithm again. Then, this results proves that the rationale behind the design of

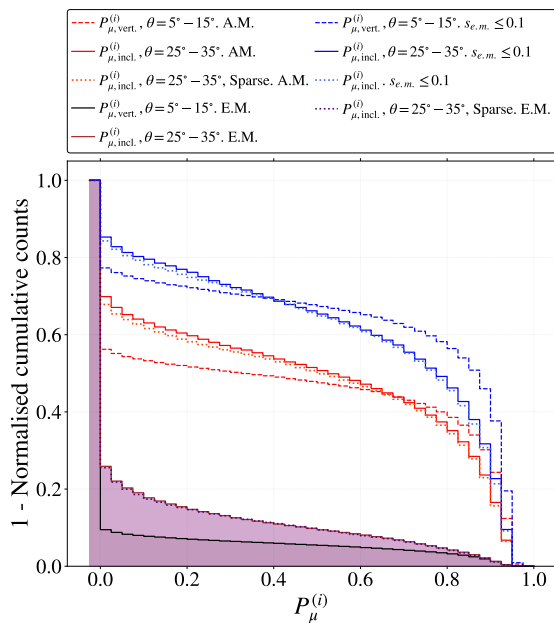


Figure 9: Normalised inverse cumulative function of the probability  $P_{\mu}^{(i)}$  of stations from proton-induced events with  $\theta_0 \in [5^{\circ}; 15^{\circ}]$  (dense array) and  $\theta_0 \in [25^{\circ}; 35^{\circ}]$  (dense and sparse array).

the station also works for these events and has a low dependence on the shower zenith angle.

From this results we can conclude that the algorithms should be trained using events that are similar to those to be analysed. Studies with greater energies are out of the scope of this article since the physics of the problem would change significantly (e.g. more than one muon crossing through a station or greater electromagnetic contamination).

## 8 Conclusions

In this work, we have shown that a WCD with a water volume of  $12\text{ m}^2 \times 1.7\text{ m}$  and 4 PMTs can be used to efficiently tag muons. For that, a machine learning-based analysis, which processes the PMT acquired signals, has been developed. The analysis has been developed using WCD events solely from proton-induced showers with  $E_0 \sim 4\text{ TeV}$  and zenith angles of  $\theta_0 \sim 10^{\circ}$  for nearly vertical showers and  $\theta_0 \sim 30^{\circ}$  for inclined showers.

In this paper, we show that the identification of the muon in the station, given as a probability,  $P_{\mu}^{(i)} \in [0; 1]$ , depends on the amount of electromagnetic contamination in the station, with nearly no dependence on the configuration of the WCD array (dense vs sparse). The proposed method was effective for both vertical and

inclined induced events, where roughly the 70% of stations with slightly contaminated muons and the 50% of all stations with muons had  $P_{\mu}^{(i)} > 0.5$ . For inclined events, just 10% of the stations without muons had  $P_{\mu}^{(i)} > 0.5$ , while for vertical events the same happens for  $P_{\mu}^{(i)} > 0$ .

Using a simple gamma/hadron discrimination observable created from  $P_{\mu}^{(i)}$  it has been shown that it is possible to distinguish between gamma and proton-induced showers with a  $S/\sqrt{B} \sim 4$  for shower energies of  $E_0 \sim 1\text{ TeV}$  and  $\theta_0 \sim 10^{\circ}$ . Moreover, it has been shown that a calibration between  $P_{\mu}$  and  $N_{\mu}$  can be built, leading to a negligible bias for  $N_{\mu} > 10$  and resolutions of  $\sim 20\%$ .

**Acknowledgements** We would like to thank to A. Bueno for all the support and useful discussions during the development of this work. The authors thank also for the financial support by OE - Portugal, FCT, I. P., under project PTDC/FIS-PAR/29158/2017. R. C. is grateful for the financial support by OE - Portugal, FCT, I. P., under DL57/2016/cP1330/cT0002. B.S.G. is grateful for the financial support by grant LIP/BI - 14/2020, under project IC&DT, POCI-01-0145-FEDER-029158.

## References

1. B. Degrange, G. Fontaine, *Comptes Rendus Physique* **16**(6-7), 587 (2015)
2. A. De Angelis, M. Pimenta, *Introduction to particle and astroparticle physics: multimessenger astronomy and its particle physics foundations* (Springer, 2018)
3. W. Atwood, A.A. Abdo, M. Ackermann, W. Althouse, B. Anderson, M. Axelsson, L. Baldini, J. Ballet, D. Band, G. Barbiellini, et al., *The Astrophysical Journal* **697**(2), 1071 (2009)
4. B. Bartoli, P. Bernardini, X. Bi, I. Bolognino, P. Branchini, A. Budano, A.C. Melcarne, P. Camarri, Z. Cao, R. Cardarelli, et al., *The Astrophysical Journal* **779**(1), 27 (2013)
5. F. Assunção, J. Correia, R. Conceição, M.J.M. Pimenta, B. Tomé, N. Lourenço, P. Machado, *IEEE Access* **7**, 110531 (2019)
6. S. Westerhoff, H. Collaboration, et al., *Advances in Space Research* **53**(10), 1492 (2014)
7. A. Zuñiga-Reyes, A. Hernández, A. Miranda-Aguilar, A. Sandoval, J. Martínez-Castro, R. Alfaro, E. Belmont, H. León, A.P. Vizcaya, arXiv preprint arXiv:1708.09500 (2017)
8. A. Abeysekara, et al., *Astrophys. J.* **843**(1), 39 (2017). DOI 10.3847/1538-4357/aa7555
9. X. Zuo, et al., *Nucl. Instrum. Meth. A* **789**, 143 (2015). DOI 10.1016/j.nima.2015.04.010
10. P. Abreu, et al., *Eur. Phys. J. C* **78**(4), 333 (2018). DOI 10.1140/epjc/s10052-018-5820-2
11. [swgo.org](http://swgo.org)
12. D. Heck, J. Knapp, J. Capdevielle, G. Schatz, T. Thouw, Report FZKA **6019** (1998)
13. S. Agostinelli, J. Allison, K.a. Amako, J. Apostolakis, H. Araujo, P. Arce, M. Asai, D. Axen, S. Banerjee, G.. Barrand, et al., *Nuclear instruments and methods in*

- 
- physics research section A: Accelerators, Spectrometers, Detectors and Associated Equipment **506**(3), 250 (2003)
14. J. Allison, et al., IEEE Transactions on Nuclear Science **53 No. 1**, 270 (2006)
  15. J. Allison, et al., Nuclear Instruments and Methods in Physics Research A **835**, 186 (2016)
  16. B.S. González, et al., **Submitted to Engineering Applications of Artificial Intelligence** (2021)
  17. D.P. Kingma, J. Ba, arXiv preprint arXiv:1412.6980 (2014)
  18. B.S. González, R. Conceição, B. Tomé, M. Pimenta, L. Herrera, A. Guillen, Journal of Physics: Conference Series **1603**, 012024 (2020). DOI 10.1088/1742-6596/1603/1/012024. URL <https://doi.org/10.1088/1742-6596/1603/1/012024>
  19. P. Assis, et al., Astropart. Phys. **99**, 34 (2018). DOI 10.1016/j.astropartphys.2018.02.004. [Erratum: Astropart.Phys. 101, 36–36 (2018)]
  20. A. Abeysekara, et al., Astrophys. J. **841**(2), 100 (2017). DOI 10.3847/1538-4357/aa729e